MATHEMATICAL BIOSCIENCES
AND ENGINEERING
Volume **10**, Number **4**, August **2013**

doi:10.3934/mbe.2013.10.997

pp. **997–1015**

MODELING OF THE MIGRATION OF ENDOTHELIAL CELLS ON BIOACTIVE MICROPATTERNED POLYMERS

Thierry Colin

Univ. Bordeaux, IMB, UMR 5251, F-33400 Talence, France

Marie-Christine Durrieu

INSERM, IECB, UMR 5248, F-33607 Pessac, France

Julie Joie

Univ. Bordeaux, IMB, UMR 5251, F-33400 Talence, France

Yifeng Lei

Univ. Bordeaux, IECB, UMR 5248, F-33607 Pessac, France

Youcef Mammeri and Clair Poignard

INRIA, F-33400 Talence, France

Olivier Saut

CNRS, IMB, UMR 5251, F-33400 Talence, France

(Communicated by Qing Nie)

Abstract. In this paper, a macroscopic model describing endothelial cell migration on bioactive micropatterned polymers is presented. It is based on a system of partial differential equations of Patlak-Keller-Segel type that describes the evolution of the cell densities. The model is studied mathematically and numerically. We prove existence and uniqueness results of the solution to the differential system. We also show that fundamental physical properties such as mass conservation, positivity and boundedness of the solution are satisfied. The numerical study allows us to show that the modeling results are in good agreement with the experiments.

1. **Introduction.** Tissue engineering is the use of combination of cells, engineering, materials, and suitable biochemical factors to improve or replace biological functions [26]. The main challenge of this scientific field consists in providing functional microvascular networks which are able to supply tissue with nutrients and oxygen and to remove metabolic wastes [18]. The lack of vascularization hampers the survival of engineered tissues after implantation [18]. Researchers rely on the increasing knowledge of angiogenic and vasculogenic processes to stimulate vascular network formation [31, 32]. This complex process of new blood vessel formation is orchestrated by the interaction between endothelial cells (ECs) and their neighboring mural cells via a complex network of intracellular signaling mechanisms [17, 28].

2010 *Mathematics Subject Classification.* Primary: 92B05, 92C17.

Key words and phrases. Tissue engineering, Keller-Segel type model, endothelial cells migration.

The authors wish to thanks the GIS AMA "Advanced Materials in Aquitaine" (http://www.ama-materials.com/) for its financial support.

Ever since the introduction of the *in vitro* experimental models of angiogenesis [11], there has been an increasing research interest to understand the intricate process of tube formation. Although many efforts have been made, the mechanism associated with angiogenesis and vascularization is still poorly understood. A deeper comprehension of cells-biomaterials interaction is then required for basic understanding of angiogenesis and vascularization in tissue engineering [5].

One strategy in developing clinical implants consists of appropriate utilizations of bioactive materials: bioactive materials may induce *in vivo* regenerative response at the site of damage, whereas when used *in vitro*, they can stimulate the tissue growth for subsequent implantation [2, 23]. Different bioactive ligands have been used to study their effects on cell functions for a better understanding of vascularization [31]. In the aim of promoting angiogenesis in the case of tissue engineering or of inhibiting angiogenesis in the case of cancer, it is important to understand the mechanisms that regulate lumen formation. Successful micropatterning of cells is becoming a key component of this field [16]. Researchers are now interested in the behavior of cells on substrates that have been patterned by micro– or nano–fabrication [10, 27]. It is known that cell positioning and physiology can be controlled by the substrate on which the cells adhere [6]. Our experiments show that the use of cell adhesion peptides that are micropatterned onto material makes possible the formation of tube-like structures unlike the use of virgin or homogeneously grafted materials [22, 23].

Actually, experimental studies using micropatterned substrates revealed that the cell migration is governed by the geometry of patterns. Endothelial cells so cultured form extensive cell-cell interactions. In some configurations, accumulation of endothelial cell junctions implies that some cells form tube-like structures. The goal of the present paper is to provide a model that describes such experimental results.

Adhesive areas are composed of cell adhesion peptides or growth factor peptides that make the cells adhere. These areas are surrounded by non-adhesive areas [22]. We assume (and this is actually confirmed by experiments) that active principles (cell adhesion peptides or growth factors) do not diffuse. Therefore endothelial cells located outside the adhesive areas cannot straightforwardly "feel" the active principles. They find out the adhesive areas indirectly. We do not consider the influence of nutrients and assume that cells obtain enough nutrients from the material (due to grafted active principles onto material). Endothelial cells are seeded onto micropatterned bioactive materials for several hours, then the unadherent cells are removed by rinsing with culture medium. Only the adhered endothelial cells remain on the material. The initial cell density is around 40 000 cells per cm^2. At the beginning of the experiments, during the migration phase, we observe that cells have a random motility and stop on adhesive areas. Moreover the attraction of endothelial cells on adhesive areas seems to be higher than the attraction of cells located outside these areas. Experiments show that endothelial cells are grouping together along the micropatterns. On bioactive materials composed of thin strips of tens of micrometers width, that is the order of magnitude of cell size, endothelial cells line their cytoskeleton to adjust themselves with the bioactive micropattern. Note also that tubes containing a central lumen may appear for such micropatterns [23, 7]. In other words, blood vessels are created from an initial random density of endothelial cells. Such phenomenon is not observed with larger strips [7, 20, 25].

To illustrate these experiments, we present in Fig. 1 pictures of the micropatterned bioactive materials at the end of the migration phase. Two different micropatterns are considered: on Fig. 1(a) thin adhesive areas (bioactive pattern size: 10 μm and distance between patterns: 100 μm) have beed used, whereas Fig. 1(b) shows the end of the migration on large strips (bioactive pattern size: 300 μm and distance between patterns: 100 μm). We refer the reader to [22, 23] for a detailed description of these experiments.

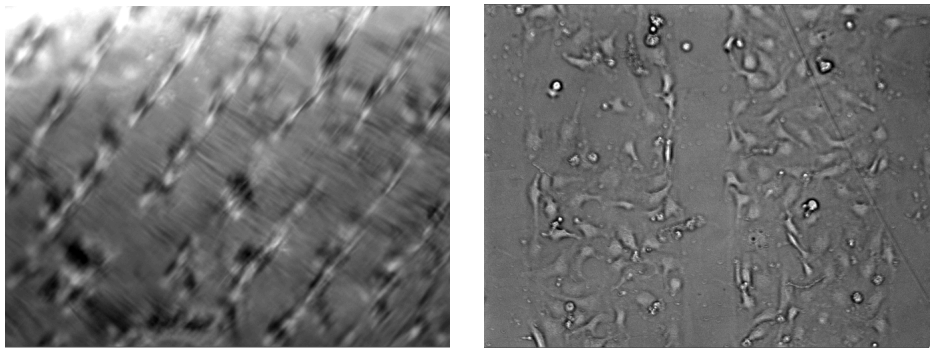

(a) thin areas (b) large areas

FIGURE 1. Endothelial cell alignment onto micropatterned polymer (PET) (10μm (A) and 300 μm (B) stripes of SVVYGLR peptides) [22]. The distance between bioactive patterns is 100 μm.

We observed that for the large adhesive areas, the adhered cell density is smaller than for thin strips. Therefore the geometry of the micropatterns is crucial in the endothelial cell migration and thus, in the formation of new vessels.

In this paper, we are interested in understanding how these patterns (size and spacing of the bioactive microfeatures) do influence endothelial cell migration. The model we present here is a Patlak-Keller-Segel type model [1, 13, 21, 30]. The chemotaxis term takes the cell-cell interactions into account instead of the cell-chemical attractant interactions. We show that this new model based on a system of coupled partial differential equations satisfies the mass conservation law and that existence and uniqueness results of weak solution hold. We also provide numerical results in accordance with the experiments, which ensures the validity of our model. Moreover, these numerical simulations make possible to obtain informations on the influence of the geometry and of the initial concentration of cells on the cell migration.

The outline of the article is the following. In section 2 we describe the mathematical model and we state the main result of global existence and uniqueness of the weak solution to the P.D.E system. Section 3 is devoted to the proof of the main theorem. We then provide numerical results in section 4 in order to compare the simulations to the experiments.

2. **Description of the model and main result.**

In this section, we describe the Patlak-Keller-Segel type model we study throughout the paper. The model is

composed of a diffusion term coupled with a reaction term, that describes the effect of the chemoattractants, which statisfy a diffusion equation.

Various continuous models of Patlak-Keller-Segel type have been used to describe cell motility [21, 30, 4, 14, 8, 33]. The governing equations of these models are written in the following general form, in a domain $\Omega \subset \mathbb{R}^n$:

$$\begin{aligned} \partial_t u &= \nabla.\left(D_1(u,v)\nabla u - \chi(u,v)u\nabla v\right) + f(u,v) \quad \text{on } \Omega, \\ \partial_t v &= \nabla.\left(D_2(u,v)\nabla v\right) + g(u,v) - h(u,v)v \qquad \text{on } \Omega, \end{aligned}$$

where u denotes the cells density, v is the chemical signal concentration. The diffusive terms take the random cell motility into account, whereas the advection describes the influence of the chemical signal on the cell motion. The two corresponding diffusion parameters are denoted by D_1 and D_2, while χ is the chemotaxis coefficient. The function f describes the growth and the death of cells, whereas the functions g and h describe respectively the production and the degradation of the chemotaxic signal. These equations have been theoretically studied for several years [3, 4, 8, 12, 14, 33]. Based on this extensive literature, we provide a slightly modified model to describe the cell migration on bioactive micropatterns.

2.1. **Statement of the equations.** According to the experiments, the behavior of the cells is drastically different on the adhesive areas and outside these areas. Actually, outside the adhesive strips, the cells seem to attract each other (probably thanks to the chemoattractant they produce) and also diffuse randomly in the domain, but as soon as they reach the adhesive strips the cells seem stuck on the strips and then they diffuse only on the bioactive material, ignoring the outer cells. Moreover, it seems that the cells located on the adhesive strips produce more chemoattractant than the outer cells.

Since there is no clear understanding of the way that endothelial cells communicate, we chose to consider the chemotaxis term as the attraction between endothelial cells (and we do not consider any gradient of concentration of the chemoattractant).

Based on these assumptions, we derive the following model. Consider a domain Ω splitted between adhesive areas, denoted by $\widetilde{\Omega}$, and non-adhesive areas denoted by $\Omega \setminus \widetilde{\Omega}$. We assume that all the domains are bounded domains with smooth boundary.

Two different types of endothelial cells are considered. We denote by $u_1(t,x,y)$ the density of endothelial cells, at any point (x,y) and at time t, that can freely move (*i.e.* they have yet to move over adhesion proteins). Cells that are adhering on the substrate are tracked through their density u_2. The function v represents the density of the chemoattractant. The equations governing the endothelial cell migration are given for $t > 0$ by

$$\partial_t u_1 = d_1 \Delta u_1 - \lambda \mathbb{1}_{\widetilde{\Omega}} u_1(1-u_2) - \nabla.\left(\chi(u_1,v)u_1\nabla v\right), \qquad \text{in } \Omega, \tag{1a}$$

$$\partial_t u_2 = d_2 \Delta u_2 + \lambda \mathbb{1}_{\widetilde{\Omega}} u_1(1-u_2), \qquad \text{in } \widetilde{\Omega}, \tag{1b}$$

$$\partial_t v = \Delta v - \eta v + \gamma_1 u_1 + \gamma_2 u_2, \qquad \text{in } \Omega, \tag{1c}$$

with the homogeneous boundary conditions on $\partial\Omega$ and $\partial\widetilde{\Omega}$:

$$\partial_{\mathbf{n}} u_1|_{\partial\Omega} = 0, \quad \partial_{\mathbf{n}} u_2|_{\partial\widetilde{\Omega}} = 0, \quad \partial_{\mathbf{n}} v|_{\partial\Omega} = 0, \tag{1d}$$

and with the initial conditions $(u_1^0, u_2^0, 0)$:

$$u_1|_{t=0} = u_1^0, \quad u_2|_{t=0} = u_2^0, \quad v|_{t=0} = 0. \tag{1e}$$

We then denote by u the total cell density:

$$u(t,x) = u_1(t,x) + u_2(t,x), \quad t \geq 0,\, x \in \Omega,$$

where u_2 is extended by 0 in $\Omega \setminus \widetilde{\Omega}$.

The parameters d_1, d_2, η, γ_1, γ_2 and λ are strictly positive and they will be fitted by the experiments in a forthcoming work, but we consider here that they are given constants. The coefficients d_1 and d_2 denote the diffusion coefficients of the cells u_1 and u_2 respectively. The coefficient $\eta > 0$ is the self-degradation rate of the chemoattractant produced by the cells, while the coefficients γ_1 and γ_2 are the coefficients of the production of the chemoattractant respectively for the cell u_1 and u_2. The parameter λ is the speed with which u_1 become u_2, when u_1 lies in the bioactive micropatterns $\widetilde{\Omega}$. The first two equations describe the cell migration in Ω. Outside the bioactive strips, the endothelial cells diffuse and attract the neighboring cells via the chemotaxis sensitivity function :

$$\chi(u_1, v) = \chi^0 \frac{v}{1+|v|}(1-u_1), \quad \text{with } \chi^0 > 0.$$

Here above, χ^0 is a chemotaxis parameter, and the term $(1-u_1)$ is settled to prevent the overcrowding of the cells u_1. Endothelial cells once they reach the adhesive area $\widetilde{\Omega}$ are captured and then diffuse only in the strip. This is handled by the penalty term $-\lambda \mathbb{1}_{\widetilde{\Omega}} u_1(1-u_2)$. Cells on the strips still have a random motility and their concentration grows up as the term $\lambda \mathbb{1}_{\widetilde{\Omega}} u_1(1-u_2)$, where $1-u_2$ prevents the blow-up of u_2 in equation (1b). The third equation (1c) describes the production of the chemoattractant by the cells. Since the cells on the strip seem to be more attractive, we suppose that the production coefficients satisfy $0 < \gamma_1 < \gamma_2$. We also add a degradation coefficient $\eta > 0$ describing the metabolization of the chemoattractant.

2.2. **Main theoretical result.** We have the following theorem which is a straightforward consequence of the results of section 3:

Theorem 2.1. *Let d_1, d_2, η, γ_1, γ_2 and λ be strictly positive constants. Suppose that the initial data $(u_1^0, u_2^0) \in L^\infty(\Omega) \times L^\infty(\widetilde{\Omega})$ are such that*

$$\forall x \in \Omega, \quad 0 \leq u_1^0(x) \leq 1, \quad \forall x \in \widetilde{\Omega}, \quad 0 \leq u_2^0(x) \leq 1.$$

There exists a unique weak solution (u_1, u_2, v) to problem (1) such that

$$(u_1, u_2, v) \in L^\infty\Big([0,+\infty); L^\infty(\Omega)\Big) \times L^\infty\Big([0,\infty); L^\infty(\widetilde{\Omega})\Big) \times L^\infty\Big([0,\infty); L^\infty(\Omega)\Big),$$

and for almost any $t > 0$

$$0 \leq u_1(t,\cdot) \leq 1, \quad 0 \leq u_2(t,\cdot) \leq 1, \quad \textit{and} \quad 0 \leq v(t,\cdot) \leq \frac{1}{\eta}\left(\gamma_1 + \gamma_2\right).$$

The next section is devoted to prove this theorem. The proof is based on Gaussian upper bounds for heat kernels [29]–[35].

3. **Theoretical study of the model .** In this section we study the mathematical properties of the model. Throughout this section we suppose that $\widetilde{\Omega}$ and Ω are smooth domains of $\mathbb{R}^2$. We remind that d_1, d_2 and η are strictly positive coefficients.

3.1. **Kernels of the operators.** The aim of this paragraph is to provide estimates satisfied by the kernels of the operators $\partial_t - \Delta + \eta$ and $\partial_t - d_1\Delta$ in Ω and by the kernel of $\partial_t - d_2\Delta$ in $\widetilde{\Omega}$, with homogeneous Neumann conditions imposed respectively on $\partial\Omega$ and $\partial\widetilde{\Omega}$.

Definition 3.1. The kernels $\mathcal{B}$, $\mathcal{G}$ and $\widetilde{\mathcal{G}}$ of the respective operators $\partial_t - \Delta + \eta$, $\partial_t - d_1\Delta$ on Ω, and $\partial_t - d_2\Delta$ on $\widetilde{\Omega}$, all with homogeneous Neumann conditions, are respectively defined by

$$\forall (x,y) \in \Omega, \quad \lim_{t\to 0^+} \mathcal{B}(t,x,y) = \delta_y(x),$$

and for any $(t,y) \in (0,\infty)\times\Omega$,

$$\begin{cases} \partial_t \mathcal{B}(t,x,y) = \Delta \mathcal{B}(t,x,y) - \eta \mathcal{B}(t,x,y), & \forall x \in \Omega, \\ \partial_{\mathbf{n}} \mathcal{B}(t,x_{\partial\Omega},y) = 0, & \forall x_{\partial\Omega} \in \partial\Omega, \end{cases} \tag{2a}$$

for $\mathcal{B}$, while $\mathcal{G}$ is given by

$$\forall (x,y) \in \Omega, \quad \lim_{t\to 0^+} \mathcal{G}(t,x,y) = \delta_y(x), \tag{3a}$$

and for any $(t,y) \in (0,\infty)\times\Omega$,

$$\begin{cases} \partial_t \mathcal{G}(t,x,y) = d_1 \Delta \mathcal{G}(t,x,y), & \forall x \in \Omega, \\ \partial_{\mathbf{n}} \mathcal{G}(t,x_{\partial\Omega},y) = 0, & \forall x_{\partial\Omega} \in \partial\Omega, \end{cases} \tag{3b}$$

and $\widetilde{\mathcal{G}}$ is the solution to

$$\forall (x,y) \in \widetilde{\Omega}, \quad \lim_{t\to 0^+} \widetilde{\mathcal{G}}(t,x,y) = \delta_y(x), \tag{4a}$$

and for any $(t,y) \in (0,\infty)\times\widetilde{\Omega}$,

$$\begin{cases} \partial_t \widetilde{\mathcal{G}}(t,x,y) = d_2 \Delta \widetilde{\mathcal{G}}(t,x,y), & \forall x \in \widetilde{\Omega}, \\ \partial_{\mathbf{n}} \widetilde{\mathcal{G}}(t,x_{\partial\widetilde{\Omega}},y) = 0, & \forall x_{\partial\widetilde{\Omega}} \in \partial\widetilde{\Omega}. \end{cases} \tag{4b}$$

Note that the above kernels are symmetric in their second and third variables.

Proposition 1. *For any $y \in \Omega$ (respectively for any $y \in \widetilde{\Omega}$), we have the following estimates for positive constants C_Ω and $C_{\widetilde{\Omega}}$, which depend on the domain Ω and $\widetilde{\Omega}$ respectively:*

$$\|\mathcal{G}(t,\cdot,y)\|_{L^1(\Omega)} \le C_\Omega, \tag{5a}$$

$$\left\|\widetilde{\mathcal{G}}(t,\cdot,y)\right\|_{L^1(\Omega)} \le C_{\widetilde{\Omega}}, \tag{5b}$$

$$\|\mathcal{B}(t,\cdot,y)\|_{L^1(\Omega)} \le C_\Omega, \tag{5c}$$

and gradient estimates hold too:

$$\|\nabla_x \mathcal{G}(t,\cdot,y)\|_{L^1(\Omega)} \le C_\Omega \max(1, t^{-3/4}), \tag{6a}$$

$$\left\|\nabla_x \widetilde{\mathcal{G}}(t,\cdot,y)\right\|_{L^1(\Omega)} \le C_{\widetilde{\Omega}} \max(1, t^{-3/4}), \tag{6b}$$

$$\|\nabla_x \mathcal{B}(t,\cdot,y)\|_{L^1(\Omega)} \le C_\Omega \max(1, t^{-3/4}). \tag{6c}$$

In addition due to the boundedness of Ω*, we also have*

$$\|\nabla_y \mathcal{G}(t,\cdot,y)\|_{L^1(\Omega)} \le C_\Omega \max(1, t^{-3/4}), \tag{7a}$$

$$\left\|\nabla_y \widetilde{\mathcal{G}}(t,\cdot,y)\right\|_{L^1(\Omega)} \le C_{\widetilde{\Omega}} \max(1, t^{-3/4}), \tag{7b}$$

$$\|\nabla_y \mathcal{B}(t,\cdot,y)\|_{L^1(\Omega)} \le C_\Omega \max(1, t^{-3/4}). \tag{7c}$$

Proof. Obviously the diffusion coefficients d_1 and d_2, since they are strictly positive constants, do not play a crucial role, and can be supposed to be equal to 1, after an appropriate rescaling of the time variable t. Moreover it is sufficient to prove the above estimates for the heat kernel $\mathcal{G}$, since

$$\mathcal{B} = \mathrm{e}^{-\eta t}\mathcal{G}.$$

For $t \ge 1$, estimates (3.2)–(3.3) of [35] straightforwardly provide the result. Suppose that $0 < t \le 1$. Estimates (5) easily come from Theorem 6.10 pp 171 of [29], since for any $x \in \Omega$,

$$0 \le \frac{1}{\sqrt{t}} \int_\Omega \mathrm{e}^{-|x-y|^2/t}\, dy \le 2\pi.$$

Estimates (6) are consequences of the section 6.6 entitled Weighted Gradient Estimates and in particular of Theorem 6.19 p 185 [29]. Actually by Cauchy-Schwarz inequality

$$\begin{aligned}
\|\nabla_x \mathcal{G}(t,\cdot,y)\|^2_{L^1(\Omega)} &\le \int_\Omega |\nabla_x \mathcal{G}(t,\cdot,y)|^2\, \mathrm{e}^{2\beta|x-y|^2/t}\, dy \int_\Omega \mathrm{e}^{-2\beta|x-y|^2/t}\, dy \\
&\le Ct^{-2}\mathrm{e}^{ct} \int_\Omega \mathrm{e}^{-2\beta|x-y|^2/t}\, dy, \\
&\le 2\pi C t^{-3/2}\mathrm{e}^{ct} \le Ct^{-3/2},
\end{aligned}$$

hence the estimates (6).

Now let $\phi \in L^\infty(\Omega)$, by estimates (6) and since the measure $|\Omega|$ of Ω is bounded we infer

$$\begin{aligned}
\int_\Omega |\phi(y)| \int_\Omega |\nabla_y \mathcal{G}(t,x,y)|\, dx\, dy &= \int_{\Omega\times\Omega} |\phi(y)|\, |\nabla_y \mathcal{G}(t,x,y)|\, dy\, dx, \\
&\le \|\phi\|_{L^\infty(\Omega)} \int_\Omega \|\nabla_y \mathcal{G}(t,x,\cdot)\|_{L^1(\Omega)}\, dx, \\
&\le |\Omega| C t^{-3/4} \|\phi\|_{L^\infty(\Omega)},
\end{aligned}$$

hence estimates (7), which ends the proof of the proposition. □

Remark 1. The above estimates are probably not optimal, since for the half-plane the heat kernel writes:

$$\mathcal{G}(t,x,y) = \frac{1}{4\pi t}\left(\mathrm{e}^{|x-y|^2/(4t)} + \mathrm{e}^{|x-y^c|^2/(4t)}\right), \quad \text{where } y^c = (y_1, -y_2),$$

and therefore the power $t^{-3/4}$ has to be replaced by $t^{-1/2}$ similarly to the heat kernel of the whole plane $\mathbb{R}^2$. However these results are sufficient to prove existence and uniqueness of the solution to problem (1).

Corollary 1. *In particular, for $T > 0$, and for any $\phi \in L^\infty([0,T];L^\infty(\Omega))$ the solution to the following problem:*

$$\begin{cases} \partial_t u = \Delta u - \eta u + \phi(t,\cdot), & \text{in } \Omega, \\ \partial_{\mathbf{n}} u|_{\partial\Omega} = 0, \quad u|_{t=0} = 0, \end{cases} \tag{8}$$

satisfies almost everywhere in $(0,T)\times\Omega$:

$$|\nabla u(t,\cdot)| \leq C_\Omega t^{1/4} \sup_{s\in(0,T)} \|\phi(s,\cdot)\|_{L^\infty(\Omega)}. \tag{9}$$

Proof. Since

$$u(t,\cdot) = \int_0^t \int_\Omega \mathcal{B}(t-s,\cdot,y)\phi(s,y)\,dy,$$

and thus

$$\begin{aligned} |\nabla u(t,x)| &\leq \int_0^t \int_\Omega |\nabla_x \mathcal{B}(t-s,x,y)\phi(s,y)|\,dy, \\ &\leq \sup_{s\in(0,T)} \|\phi(s,\cdot)\|_{L^\infty(\Omega)} \int_0^t \|\nabla_x \mathcal{B}(t-s,x,\cdot)\|_{L^1(\Omega)}, \end{aligned}$$

inequality (9) holds. □

3.2. **Local existence.** Using the above appropriate kernels, we deduce that a weak solution to problem (1) writes:

$$\begin{aligned} u_1(t,x) = &\int_\Omega \mathcal{G}(t,x,y)u_1^0(y)\,dy - \lambda \int_0^t \int_{\widetilde{\Omega}} \widetilde{\mathcal{G}}(t-s,x,y)u_1(s,y)(1-u_2)(s,y)\,dy\,ds \\ &+ \int_0^t \int_\Omega u_1(s,y)\chi(u_1,v)(s,y)\nabla_y \mathcal{G}(t-s,x,y)\cdot\nabla v(s,y)\,dy\,ds, \end{aligned} \tag{10a}$$

$$u_2(t,x) = \int_{\widetilde{\Omega}} \widetilde{\mathcal{G}}(t,x,y)u_2^0(y)\,dy + \lambda \int_0^t \int_{\widetilde{\Omega}} \widetilde{\mathcal{G}}(t-s,x,y)u_1(s,y)(1-u_2)(s,y)\,dy\,ds, \tag{10b}$$

$$v(t,x) = \int_0^t \int_\Omega \mathcal{B}(t-s,x,y)\left(\gamma_1 u_1(s,y) + \gamma_2 u_2(s,y)\right)\,dy\,ds. \tag{10c}$$

In this paragraph we aim at proving a local-existence result.

3.2.1. *Definition of the appropriate functional space $\mathcal{X}_M^T$.* Let M be a strictly positive constant, and let $T > 0$ that will be chosen later. We define the functional space $\mathcal{X}_M^T$ as

$$\mathcal{X}_M^T = \left\{ \Lambda \in L^\infty\left([0,T];L^\infty(\Omega)\right) \,:\, \sup_{t\in[0,T]} \|\Lambda(t,\cdot)\|_{L^\infty(\Omega)} \leq M \right\}.$$

Let $\mathcal{L}$ be the linear operator defined on $\mathcal{X}_M^T \times \mathcal{X}_M^T$ by

$$\mathcal{L} \,:\, (\nu_1,\nu_2) \mapsto \int_0^t \int_\Omega \mathcal{B}(t-s,\cdot,y)\left(\gamma_1\nu_1(s,y) + \gamma_2\nu_2(s,y)\right)\,dy\,ds.$$

Using estimates (5)–(6) we infer that for any $(\nu_1,\nu_2) \in \mathcal{X}_M^T \times \mathcal{X}_M^T$:

$$\begin{aligned} &\|\mathcal{L}(\nu_1,\nu_2)(t,\cdot)\|_{L^\infty(\Omega)} \leq C_\Omega(\gamma_1+\gamma_2)M, \\ &\|\nabla\mathcal{L}(\nu_1,\nu_2)(t,\cdot)\|_{L^\infty(\Omega)} \leq C_\Omega(\gamma_1+\gamma_2)Mt^{1/4}. \end{aligned} \tag{11}$$

Define now the operator $\mathcal{T}$ on $\mathcal{X}_M^T \times \mathcal{X}_M^T$ by

$$\mathcal{T} : (\nu_1, \nu_2) \mapsto \Big(\big(\mathcal{T}_1 - \mathcal{T}_2\big)(\nu_1, \nu_2)\,,\, \mathcal{T}_2(\nu_1, \nu_2) \Big),$$

where $\mathcal{T}_1$ is the operator defined on $\mathcal{X}_M \times \mathcal{X}_M^T$ by

$$\mathcal{T}_1(\nu_1, \nu_2) = \int_0^t \int_\Omega \nu_1 \chi\left(\nu_1, \mathcal{L}(\nu_1, \nu_2)\right) \nabla_y \mathcal{G}(t-s, \cdot, y) \cdot \nabla_y \mathcal{L}(\nu_1, \nu_2)\, dy\, ds,$$

and $\mathcal{T}_2$ is defined by

$$\mathcal{T}_2(\nu_1, \nu_2) = \lambda \int_0^t \int_{\widetilde{\Omega}} \widetilde{\mathcal{G}}(t-s, x, y) \nu_1(s, y)(1 - \nu_2)(s, y)\, dy\, ds.$$

Remark 2. Proving that $\mathcal{T}$ is a contraction mapping from $\mathcal{X}_M^T \times \mathcal{X}_M^T$ onto itself for small enough time T will then ensure the local existence of the weak solution given by (10) to problem (1).

3.2.2. *Contraction mappings.*

Proposition 2. *The operator $\mathcal{T}$ is a contraction mapping from $\mathcal{X}_M^T \times \mathcal{X}_M^T$ onto itself for T small enough.*

Proof. The proof is based on the properties of the kernels $\mathcal{B}$, $\mathcal{G}$ and $\widetilde{\mathcal{G}}$ given by Proposition 1. Thanks to estimates (5) we deduce for any $(\nu_1, \nu_2) \in \mathcal{X}_M^T \times \mathcal{X}_M^T$:

$$\|\mathcal{T}_2(\nu_1, \nu_2)\|_{L^\infty(\widetilde{\Omega})} \leq C_\Omega \lambda M(1+M)T,$$

hence for T small enough $\mathcal{T}_2$ maps $\mathcal{X}_M^T \times \mathcal{X}_M^T$ onto $\mathcal{X}_M^T$. Moreover using inequality:

$$|\nu_1(1-\nu_2) - \mu_1(1-\mu_2)| \leq (1+|\nu_2|)|\nu_1 - \mu_1| + |\nu_2||\mu_1 - \mu_2|,$$

we infer for T small enough the operator $\mathcal{T}_2$ is a contraction mapping from $\mathcal{X}_M^T \times \mathcal{X}_M^T$ onto $\mathcal{X}_M^T$.

Prove now that $\mathcal{T}_1$ is a contraction mapping from $\mathcal{X}_M^T \times \mathcal{X}_M^T$ onto $\mathcal{X}_M^T$. First observe that for any $s \in \mathbb{R}$, $|s|/(1+|s|) \leq 1$ hence for any $\nu_1 \in \mathcal{X}_M^T$, for any $s \in \mathbb{R}$,

$$\|\chi_1(\nu_1, s)(t, \cdot)\|_{L^\infty(\Omega)} \leq \chi^0(1+M), \quad \text{for almost any } t \in (0, T),$$

hence for any $(\nu_1, \nu_2) \in \mathcal{X}_M^T \times \mathcal{X}_M^T$

$$\|\chi_1(\nu_1, \mathcal{L}(\nu_1, \nu_2))(t, \cdot)\|_{L^\infty(\Omega)} \leq \chi^0(1+M), \quad \text{for almost any } t \in (0, T),$$

and thanks to estimates (6)–(11)

$$|\mathcal{T}_1(\nu_1, \nu_2)(t, \cdot)| \leq C_\Omega\, (\gamma_1 + \gamma_2)\, \chi^0 (1+M) M^2 \sqrt{T}.$$

This implies that for T small enough $\mathcal{T}_1$ maps $\mathcal{X}_M^T \times \mathcal{X}_M^T$ onto $\mathcal{X}_M^T$. In addition observe that for two couples (ν_1, ν_2) and (μ_1, μ_2) belonging to $\mathcal{X}_M^T \times \mathcal{X}_M^T$ we have

$$\begin{aligned}
&\mathcal{T}_1(\nu_1, \nu_2) - \mathcal{T}_1(\mu_1, \mu_2) \\
&= \int_0^t \int_\Omega (\nu_1 - \mu_1) \chi^{\nu_1, \nu_2} \nabla_y \mathcal{G}(t-s, \cdot, y) \cdot \nabla_y \mathcal{L}(\nu_1, \nu_2)\, dy\, ds \\
&+ \int_0^t \int_\Omega \mu_1 \chi^{\nu_1, \nu_2} \nabla_y \mathcal{G}(t-s, \cdot, y) \cdot \nabla_y \mathcal{L}(\nu_1 - \mu_1, \nu_2 - \mu_2)\, dy\, ds \\
&+ \int_0^t \int_\Omega \mu_1 \left(\chi^{\nu_1, \nu_2} - \chi^{\mu_1, \mu_2}\right) \nabla_y \mathcal{G}(t-s, \cdot, y) \cdot \nabla_y \mathcal{L}(\mu_1, \mu_2)\, dy\, ds,
\end{aligned}$$

where to simplify notations we have denoted by χ^{ν_1,ν_2} the function

$$\chi^{\nu_1,\nu_2} = \chi(\nu_1, \mathcal{L}(\nu_1,\nu_2)),$$

and similarly for χ^{μ_1,μ_2}. According to estimates (6) and thanks to the definition of $\mathcal{L}$ we infer

$$\|\nabla_y \mathcal{L}(\nu_1-\mu_1,\nu_2-\mu_2)\| \le C_\Omega(\gamma_1+\gamma_2)t^{1/4}\left(\|\nu_1-\mu_1\|_{L^\infty(\Omega)} + \|\nu_2-\mu_2\|_{L^\infty(\Omega)}\right).$$

Moreover, observing that

$$\begin{aligned}\chi^{\nu_1,\nu_2} - \chi^{\mu_1,\mu_2} &= \chi^0 \frac{\mathcal{L}(\nu_1,\nu_2)}{1+|\mathcal{L}(\nu_1,\nu_2)|}(\mu_1-\nu_1)\\ &\quad + \chi^0(1-\mu_1)\left(\frac{\mathcal{L}(\nu_1,\nu_2)}{1+|\mathcal{L}(\nu_1,\nu_2)|} - \frac{\mathcal{L}(\mu_1,\mu_2)}{1+|\mathcal{L}(\mu_1,\mu_2)|}\right),\end{aligned}$$

we deduce from estimates (5)–(6)–(7) and (11) that there exists a constant $C>0$ which depends on M, and on the parameters χ^0, γ_1, γ_2, λ such that

$$\|\mathcal{T}_1(\nu_1,\nu_2) - \mathcal{T}_1(\mu_1,\mu_2)\|_{L^\infty(\Omega)} \le C\sqrt{T},$$

which ensures the strict contractility of $\mathcal{T}_1$ for T small enough, and therefore $\mathcal{T}$ is a strict contraction from $\mathcal{X}_M^T \times \mathcal{X}_M^T$ onto itself. □

The Picard fixed point theorem straightforwardly implies the following theorem of existence and uniqueness for small time.

Theorem 3.2. *Let $(u_1^0, u_2^0) \in L^\infty(\Omega)\times L^\infty(\widetilde{\Omega})$. Then for T small enough there exists a unique weak solution (u_1,u_2,v) to (1) such that*

$$(u_1,u_2,v) \in L^\infty\left([0,T];L^\infty(\Omega)\right)\times L^\infty\Big([0,T];L^\infty(\widetilde{\Omega})\Big)\times L^\infty\Big([0,T];L^\infty(\Omega)\Big).$$

3.3. **Mass conservation and global existence.** We first observe that the total mass of cells is conserved.

Proposition 3. *Let $(u_1^0,u_2^0)\in L^\infty(\Omega)\times L^\infty(\widetilde{\Omega})$ and let T small enough so that a weak solution (10) to (1) exists. Then for any $t\in[0,T]$*

$$\int_\Omega u(t,x)\,dx = \int_\Omega (u_1 + \mathbb{1}_{\widetilde{\Omega}}\,u_2)(t,x)\,dx = \int_\Omega u_1^0\,dx + \int_{\widetilde{\Omega}} u_2^0\,dx$$

Proof. Actually integrating (1a) and (1b) respectively and summing the integrands imply, since $\partial_{\mathbf{n}}u_1|_{\partial\Omega}$, $\partial_{\mathbf{n}}u_2|_{\partial\widetilde{\Omega}}$ and $\partial_{\mathbf{n}}v|_{\partial\Omega}$ vanish

$$\partial_t \int_\Omega u(x)\,dx = \partial_t \int_\Omega (u_1(x)+u_2(x))\,dx = 0.$$

□

We now show that if u_1^0 and u_2^0 are positive and bounded by 1 then u_1 and u_2 stay positive and bounded by 1 on $[0,T]$.

Proposition 4. *Let $(u_1^0,u_2^0)\in L^\infty(\Omega)\times L^\infty(\widetilde{\Omega})$ and let T small enough so that a weak solution given by (10) to problem (1) exists. If (u_1^0,u_2^0) are such that*

$$0\le u_1^0\le 1, \quad 0\le u_2^0\le 1,$$

then for almost any $t\in[0,T]$

$$0\le u_1(t,x)\le 1, \quad 0\le u_2(t,x)\le 1.$$

In addition

$$0 \leq v(t,x) \leq \frac{1}{\eta}\left(\gamma_1 + \gamma_2\right), \quad \text{for } x \in \Omega.$$

Therefore the weak solution (10) *exists for almost any* $t \in (0, +\infty)$.

Proof. First observe that if u_1 is positive then since u_2^0 is positive the function u_2 is positive almost everywhere. Actually multiplying (1b) by $u_2^- = \max(0, -u_2)$ and integrating by parts implies

$$\frac{1}{2}\partial_t \|u_2^-(t,\cdot)\|^2_{L^2(\widetilde{\Omega})} = -d_2 \|\nabla u_2^-\|^2_{L^2(\widetilde{\Omega})} - \lambda \int_{\widetilde{\Omega}} \left(u_1 u_2^- + u_1 (u_2^-)^2\right) dx \leq 0,$$

hence u_2^- equal zero. From this, we infer that v is positive by multiplying (1c) by v^-, integrating by parts and using the well-known Gronwall lemma.

Prove now that $u_1^- = \max(0, -u_1)$ vanishes too. Multiply (1a) by u_1^- and integrate by parts to obtain for almost any $t \in [0, T]$:

$$\begin{aligned}\frac{1}{2}\partial_t \|u_1^-(t,\cdot)\|^2_{L^2(\Omega)} \leq -d_1 \|\nabla u_1^-(t,\cdot)\|^2_{L^2(\Omega)} + \lambda(1+M)\|u_1^-(t,\cdot)\|^2_{L^2(\widetilde{\Omega})} \\ + \chi^0 \left| \int_\Omega u_1^- \frac{v}{1+|v|}(1-u_1^-)\nabla v \nabla u_1^- \, dx \right|.\end{aligned}$$

Moreover applying estimates (9) to v implies

$$\begin{aligned}\left| \int_\Omega u_1^-(1-(u_1+u_2))\nabla v \nabla u_1^- \, dx \right| &\leq C_\Omega t^{1/4} \|\gamma_1 u_1(t,\cdot) + \gamma_2 \mathbb{1}_{\widetilde{\Omega}} u_2(t\cdot)\|_{L^\infty(\Omega)} \\ &\quad \times \int_\Omega u_1^-(t,x)|1-u_1^-|(t,x)\nabla u_1^-(t,x)\, dx, \\ &\leq C_\Omega T^{1/4} M(\gamma_1+\gamma_2)(1+2M) \\ &\quad \times \int_\Omega \left|u_1^-(t,x)\nabla u_1^-(t,x)\right| \, dx, \\ &\leq \widetilde{C} T^{1/4} \left(\frac{1}{4\alpha}\|\nabla u_1^-\|^2_{L^2(\Omega)} + \alpha \|u_1^-\|^2_{L^2(\Omega)} \right),\end{aligned}$$

by Cauchy-Schwarz estimates and the well-known Peetre's inequality with $\alpha > 0$ large enough. Thus, since $|s|/(1+|s|) \leq 1$ for any $s \in \mathbb{R}$, we infer

$$\partial_t \|u_1^-(t,\cdot)\|^2_{L^2(\Omega)} \leq \alpha \widetilde{C} T^{1/4} \|u_1^-(t,\cdot)\|^2_{L^2(\Omega)}.$$

Gronwall's lemma implies therefore that

$$\|u_1^-(t,\cdot)\|^2_{L^2(\Omega)} = 0,$$

since $u_1^-(0,\cdot)$ equals zero.

Prove now that $u_2 \leq 1$. Let $U_2 = u_2 - 1$:

$$\partial_t U_2 = \Delta U_2 - \lambda u_1 U_2,$$

hence, multiplying by $U_2^+ = \max(0, U_2)$ and integrating by parts the above equation lead to $\partial_t \|U_2^+\|^2_{L^2(\Omega)} \leq 0$. Since $U_2^+(0,\cdot)$ equals 0, we infer that U_2 vanishes everywhere, and therefore $u_2 \leq 1$.

Similarly let

$$U_1 = u_1 - 1.$$

Then U_1 satisfies in Ω:

$$\partial_t U_1 = d_1 \Delta U_1 - \lambda \mathbb{1}_{\widetilde{\Omega}}(1-u_2)\,(U_1+1) + \chi^0\,\nabla.\left((U_1+1)\frac{v}{1+|v|}U_1\nabla v\right). \qquad (12)$$

Once again, multiply (12) by $U_1^+ = \max(U_1, 0)$ and integrate by parts to obtain

$$\begin{aligned}\frac{1}{2}\partial_t \|U_1^+\|^2_{L^2(\Omega)} =& - d_1 \|\nabla U_1^+\|^2_{L^2(\Omega)} - \lambda \int_{\widetilde{\Omega}} (1-u_2) U_1^+ (U_1^+ + 1)\, dx \\ & - \chi^0 \int_\Omega (U_1^+ + 1)\frac{v}{1+|v|} U_1^+ \nabla v \cdot \nabla U_1^+\, dx.\end{aligned}$$

Since $1-u_2$ is positive and using Cauchy-Schwarz estimate and Peetre inequality for α large enough (as used above to prove that $u_1 \geq 0$) implies that

$$\partial_t \|U_1^+\|^2_{L^2(\Omega)} \leq \alpha\, C \|U_1^+\|^2_{L^2(\Omega)}.$$

Therefore Gronwall lemma implies that U_1^+ vanishes almost everywhere in $(0,T)\times\Omega$ hence $u_1 \leq 1$.

To obtain the positivity of v, first multiply (1c) by v^- and integrate by part to infer, since u_1 and u_2 are positive that:

$$\partial_t \|v^-\|^2_{L^2(\Omega)} \leq 0.$$

Then the function $V = v - \eta^{-1}(\gamma_1 + \gamma_2)$ satisfies

$$\partial_t V = \Delta V - \eta V + \gamma_1(u_1 - 1) + \gamma_2(u_2 - 1).$$

Since $\gamma_1(u_1-1) + \gamma_2(u_2-1) \leq 0$, we infer that V^+ identically vanishes after multiplication and integration by parts, hence

$$0 \leq v \leq \eta^{-1}(\gamma_1 + \gamma_2).$$

From the implicit representation integral of u_1 and u_2 we deduce easily that if T_M is the maximal time of existence, then there exists a sequence $(t_n)_{n\in\mathbb{N}}$ tending to T_M, with $t_n < T_M$ such that

$$\lim_{n\to+\infty} \|u_1(t_n,\cdot)\|_{L^\infty} = +\infty,$$

hence u_1 and u_2 exists for almost any $t \in (0,+\infty)$ by contraposition. □

Theorem 2.1 is an easy consequence of the above results.

The following result is a straightforward consequence of proposition 4. It ensures that the mass of the cells tends to concentrate on the micropatterns.

Corollary 2. *Let $(u_1^0, u_2^0) \in L^\infty(\Omega)\times L^\infty(\widetilde{\Omega})$ such that*

$$0 \leq u_1^0 \leq 1, \quad 0 \leq u_2^0 \leq 1,$$

and let (u_1, u_2) the weak solution to problem (1). Then

$$\begin{aligned} 0 \leq \int_\Omega u_1(t,x)\,dx \leq \int_\Omega u_1(0,x)\,dx, \\ \int_{\widetilde{\Omega}} u_2(0,x)\,dx \leq \int_{\widetilde{\Omega}} u_2(t,x)\,dx \leq |\widetilde{\Omega}|.\end{aligned}$$

4. **Numerical results.** We now describe the numerical schemes that are used to compute problem (1), and then we show the simulations that corroborate the experimental results.

4.1. **Approximation of the problem.** We consider a cartesian mesh (composed by quadrilaterals). We discretize the model using the finite volume method [9] and we use an implicit Crank-Nicolson scheme for the time discretization. We solve the model using a decoupled approach [15]. In particular, the first equation is split into advection and diffusion parts. Let us recall the expression of this equation :

$$\partial_t u_1 = d_1 \Delta u_1 - \lambda \mathbb{1}_{\widetilde{\Omega}} u_1 (1 - u_2) - \nabla . (\chi(u_1, v) u_1 \nabla v) \text{ in } \Omega. \tag{13}$$

To simplify the notations we define A and B as:

$$A(u_1, u_2) = d_1 \Delta u_1 - \lambda \mathbb{1}_{\widetilde{\Omega}} u_1 (1 - u_2), \quad \text{and} \quad B(u_1, v) = \nabla . (\chi(u_1, v) u_1 \nabla v) .$$

Let us denote the time step by Δt, set $t^n = n\Delta t$ and let (u_1^n, u_2^n, v^n) be the solution at the time t^n. At each time step we first solve the diffusive part :

$$\frac{\tilde{u}_1^{n+1} - u_1^n}{\Delta t} = \frac{1}{2} \left(A(\tilde{u}_1^{n+1}, u_2^{n+1}) + A(u_1^n, u_2^n) \right) .$$

For all the diffusive terms, the spatial discretization is handled by a centered finite volume scheme, all the species being computed at the centre of each element of the mesh. We then solve the advection part :

$$\frac{u_1^{n+1} - \tilde{u}_1^{n+1}}{\Delta t} = \frac{1}{2} \left(B(u_1^{n+1}, v^{n+1}) + B(\tilde{u}_1^{n+1}, v^n) \right) .$$

The high order WENO 5 (Weighted Essentially Non-Oscillatory) finite difference scheme introduced in [24] and improved in [19] has been used to handle the convective term. These solvers are implemented in the academic library eLYSe[1].

In the following the initial conditions write

$$u_1^0 = \mathbb{1}_{\Omega \setminus \widetilde{\Omega}} u^0, \quad u_2^0 = \mathbb{1}_{\widetilde{\Omega}} u^0, \tag{14}$$

where u^0 is a function of $x \in \Omega$. Hence the supports of u_1 and u_2 are disjoint at the initial time.

4.2. **Mathematical behavior of the model.** In this paragraph, we present the numerical results, that corroborate the mathematical results of the previous section. We want to check the properties of the model, when the maximal cell density on the adhesive area is reached. The domain Ω is the unit square $\Omega = [0, 1] \times [0, 1]$. The cartesian grid is composed by 100×100 quadrilaterals. The domain $\widetilde{\Omega}$ is the strip of width 0.08 located at the middle of Ω (cf Fig. 2).

At the initial time the cells are uniformly distributed meaning u^0 of (14) is constant. We consider two different values of u^0:

$$u^0 = \begin{cases} 0.08, \\ 0.25. \end{cases}$$

We plot the results along the axis $\{y = 0.5\}$ in order to have the profile of the distribution of u_1 and u_2. The densities u_1 along the axis at different time steps are given by Fig. 3 and the densities u_2 at the same time steps are given by Fig. 4.

When considering $u^0 = 0.08$, the maximal density on the adhesive area is never reached. We observe that u_1 is decreasing, while u_2 is increasing with respect to the time. In the second case, for $u^0 = 0.25$, the maximal density of u_2 is reached at $t = 0.3$ therefore after this time the cells u_1 cannot become u_2. As expected, the migration stops. These simulations show that a minimum amount of endothelial cells is required at the initial time in order to reach the maximal concentration on

[1] http://www.math.u-bordeaux1.fr/~osaut/

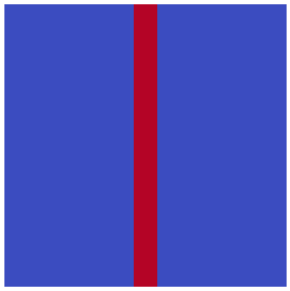

FIGURE 2. Geometry of the micropattern.

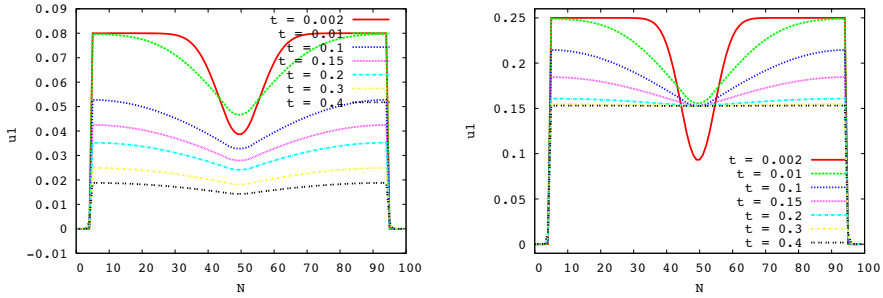

(a) Profiles of u_1 for $u^0 = 0.08$ (b) Profiles of u_1 for $u^0 = 0.25$

FIGURE 3. Profiles of $u_1(t, x, y = 0.5)$ at different time steps for two different initial conditions.

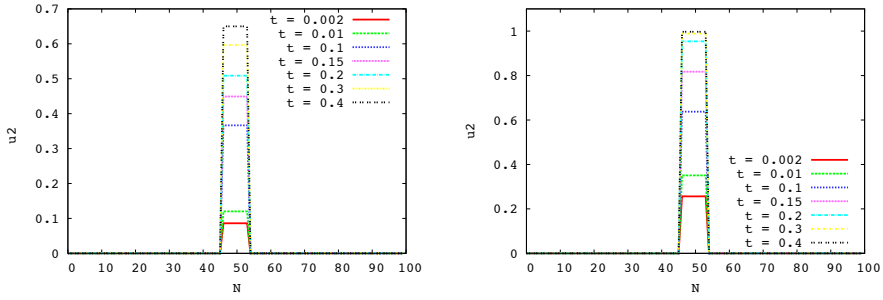

(a) Profiles of u_2 for $u^0 = 0.08$ (b) Profiles of u_2 for $u^0 = 0.25$

FIGURE 4. Behavior of $u_2(t, x, y = 0.5)$ at different time steps.

the strips at the end of the experiment. If this initial concentration is too small the final density of endothelial cells is suboptimal.

4.3. **Behavior on realistic benchmarks.** We now provide simulations in realistic setups: throughout this subsection the initial data u^0 of (14) is a normal random distribution (between 0 and 1).

4.3.1. *Behavior on the thin strips.* We first consider a bioactive micropattern composed by six adhesive thin strips (in red on Fig. 5(b)).

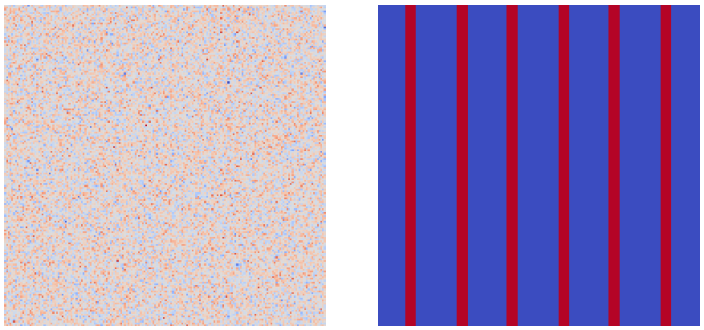

(a) The initial random distribution of endothelial cells

(b) The micropattern. Width strips = 0.05

FIGURE 5. Initial setup: endothelial cells (left) and adhesion substrate (right).

The simulation Fig. 6, represents the total density of endothelial cells ($u = u_1 + u_2$) at time $t = 0.3$ (in Fig. 6(a)) and 1.0 (in Fig. 6(b)) obtained for the following set of parameters: $d_1 = d_2 = \chi^0 = \gamma_2 = 1, \gamma_1 = 0.5, \lambda = 100$.

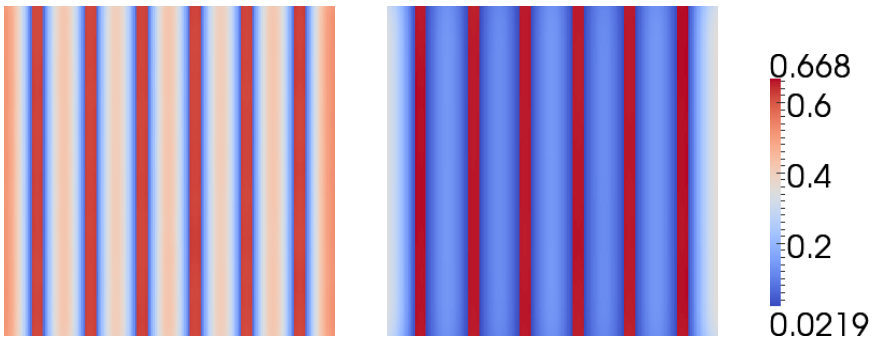

(a) t = 0.3

(b) t = 1.0

FIGURE 6. The total density of endothelial cells u at two different time steps.

Fig. 7 shows the behavior of v for the same set of parameters.

The numerical results are in good agreement with the expected evolutions. Indeed, the cell density u_2 on the adhesive areas increases with the time variable, whereas outside u_1 becomes very small. Cells are stucked on the strips and stop moving once they are over them. As a consequence the density of the attractant on the strips also increases.

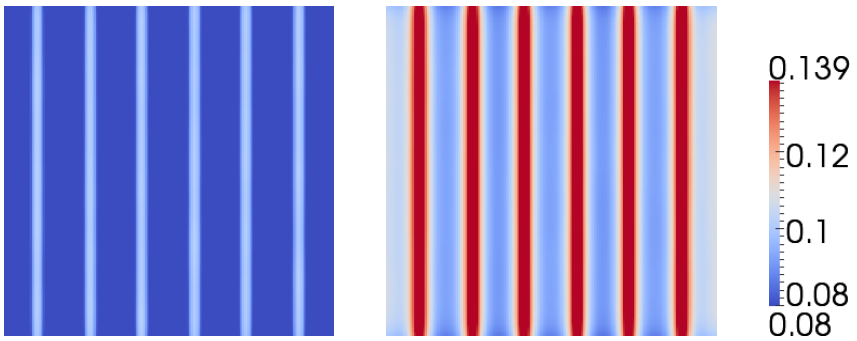

(a) t = 0.3 (b) t = 0.6

FIGURE 7. The density v at two different time steps.

4.3.2. *Behavior on large strips.* We now consider a domain $\Omega = [0,1] \times [0,1]$ composed by two large strips of length 0.2. The geometry is presented in Fig. 8(b)

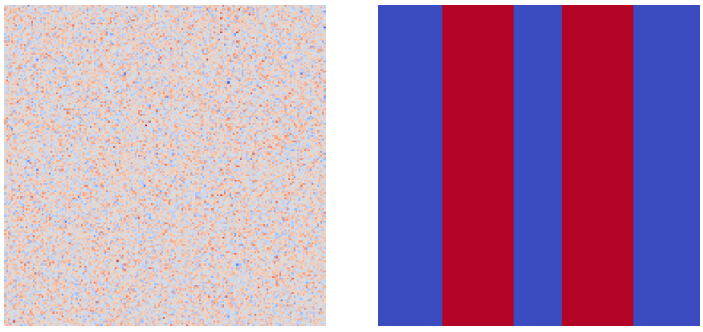

(a) The initial random distribution of endothelial cells

(b) The micropattern. Width strip = 0.2

FIGURE 8. Initial setup: endothelial cells (left) and patterns (right).

In Fig. 9, we present the total density of endothelial cells ($u = u_1 + u_2$) at times 0.3 (in Fig. 9(a)) and 1.0 (in Fig. 9(b)) obtained for the choice of parameters : $d_1 = d_2 = \chi^0 = \gamma_2 = 1, \gamma_1 = 0.5, \lambda = 100$.

In Fig. 10, we present the behavior of the chemoattractant v for the same set of parameters at the times $t = 0.3$ and $t = 0.6$.

As previously we observe a behavior in good agreement with the experiments. When considering two large adhesive areas the velocity of the migration is smaller than for a large number of thin strips. Indeed at the time step $t = 1.0$ we observe that with thin strips the migration seems to be more advanced than in the case with large strips. This could be explained by the fact that some cells are far away from a strip and their migration toward the strips takes more time.

4.3.3. *Influence of the number of strips on the migration.* We want to study the influence of the pattern spacing on the cell migration. We set the surface of the

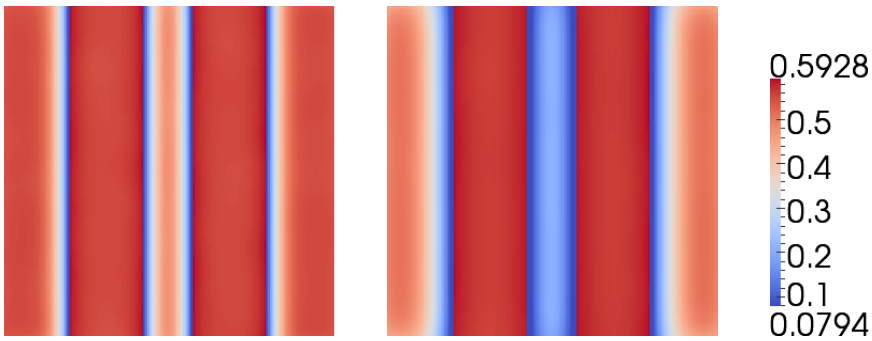

(a) t = 0.3 (b) t = 1.0

FIGURE 9. The density of endothelial cells u at two different time steps.

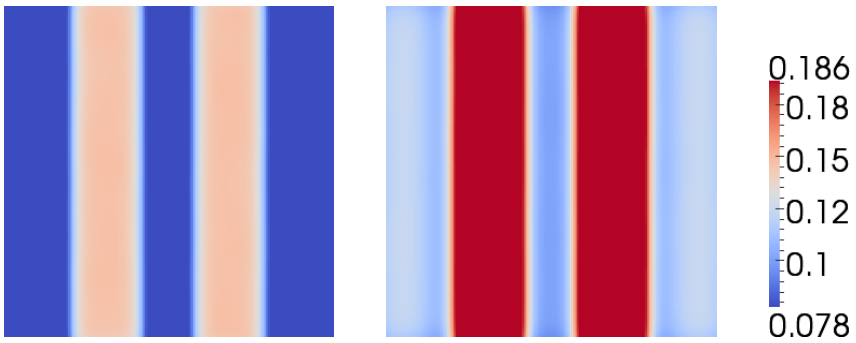

(a) t = 0.3 (b) t = 0.6

FIGURE 10. The density of the signal v at two different time steps.

adhesive domain, and let the number of strips, N_s, vary. The average of u_2 in term of the time for $N_s = 1$, 2, and 4 is presented in Fig. 11.

We observe that when considering four strips the migration is quicker. Moreover the mean density reached is higher, which corroborates the experiments.

5. **Conclusion.** In this paper a macroscopic model describing the endothelial cell migration on bioactive micropatterns is presented. Its major biological assumption is that the cells produce a chemical substance so as to gather, but the bioactive chemical substance does not diffuse any chemoattractants: it just attracts the cells to locate on it.

Mathematically, mass conservation, global existence and uniqueness results are shown. Numerically, the model behaves in good agreement with the biological experiments. Despite the lack of direct attraction of the bioactive patterns, the non-washed out endothelial cells end up on the patterns since the cells adhered on the micropatterns produce more chemoattractants than the cells outside the bioactive materials. We have observed two facts that have been reported by the experiments:

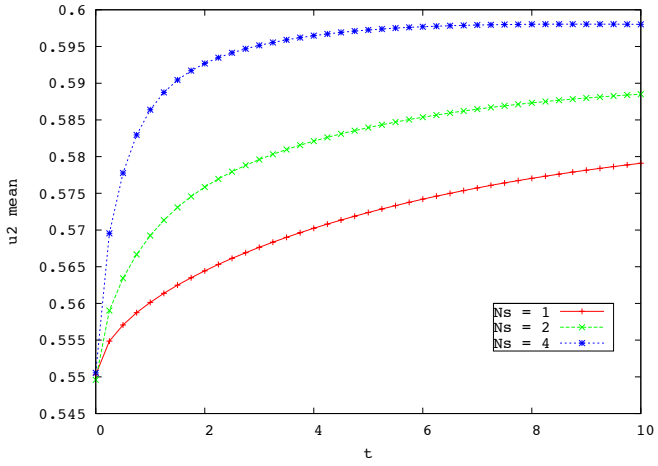

FIGURE 11. The average of the density u_2 with respect to the time for different number of strips.

1. For a given surface of bioactive material, the process of cell migration is more efficient with a large number of thin strips than with a small number of large strips.
2. There exists a minimum value of the initial density of endothelial cells to be imposed in order to have an optimal cell migration towards bioactive patterns.

We therefore believe that this model is a first step towards better understanding of cell migration on micropatterns, the long-term goal being optimal designing of patterns in order to build biological tissues.

REFERENCES

[1] A. Anderson and M. Chaplain, *Continuous and discrete mathematical models of tumor-induced angiogenesis*, Bulletin of Mathematical Biology, **60** (1998), 857–899.

[2] K. Anselme, P. Davidson, A. M. Popa, M. Giazzon, M. Liley and L. Ploux, *The interaction of cells and bacteria with surfaces structured at the nanometre scale*, Acta Biomaterialia, **6** (2010), 3824–3846.

[3] P. Biler and T. Nadzieja, *Existence and nonexistence of solutions for a model of gravitational interaction of particles*, I. Colloq. Math., **66** (1993), 319–334.

[4] A. Blanchet, J. Dolbeault and B. Perthame, *Two dimensional Keller–Segel model: Optimal critical mass and qualitative properties of the solution*, Electron. J. Differential Equations, **2006**, No. 44, 32 pp. (electronic).

[5] P. Carmeliet and M. Tessier–Lavigne, *Common mechanisms of nerve and blood vessel wiring*, Nature, **436** (2005), 193–200.

[6] C. S Chen, M. Mrksich, S. Huang, G. M. Whitesides and D. E. Ingber, *Geometric control of cell life and death*, Science, **276** (1997), 1425–1428.

[7] L. E. Dike, C. S. Chen, M. Mrksich, J. Tien, G. M. Whitesides and D. E. Ingber, *Geometric control of switching between growth, apoptosis, and differentiation during angiogenesis using micropatterned substr'ates*, in Vitro Cell. Dev. Biol., **35** (1999), 441–448.

[8] J. Dolbeault and B. Perthame, *Optimal critical mass in the two dimensional Keller-Segel model in* $\mathbb{R}^2$, C. R. Math. Acad. Sci. Paris, **339** (2004), 611–616.

[9] R. Eymard, T. Gallouet and R. Herbin, "Finite Volume Methods," Handbook of Numerical Analysis, (eds. P. G Ciarlet and J. L Lions), 2007.

[10] A. Folch and M. Toner, *Microengineering of cellular interactions*, Annu. Rev. Biomed. Eng., **2** (2000), 227–256.

[11] J. Folkman and C. Haudenschild, *Angiogenesis in vitro*, Nature, **288** (1980), 551–556.

[12] H. Gajewski and K. Zacharias, *Global behavior of a reaction-diffusion system modelling chemotaxis*, Math. Nachr., **195** (1998), 77–114.
[13] T. Hillen and K. J. Painter, *A user's guide to PDE models for chemotaxis*, J. Math. Biol., **58** (2008), 183–217.
[14] D. Horstmann, *The nonsymmetric case of the Keller-Segel model in chemotaxis: Some recent results*, Nonlinear Differ. Equ. Appl., **8** (2001), 399–423.
[15] W. Hundsdorfer and J. G. Verwer, "Numerical Solution of Time-Dependent Advection-Diffusion-Reaction Equations," Springer Series in Comput. Math., **33**, Springer, 2003.
[16] Y. Ito, *Surface micropatterning to regulate cell functions*, Biomaterials, **20** (1999), 2333–2342.
[17] R. K. Jain, *Molecular regulation of vessel maturation*, Nat. Med., **9** (2003), 685–593.
[18] R. K. Jain, P. Au, J. Tam, D. G. Duda and D. Fukumura, *Engineering vascularized tissue*, Nat Biotechnol, **23** (2005), 821–823.
[19] G. S. Jiang and C. W Shu, *Efficient implementation of weighted ENO schemes*, J. of Computational Physics, **126** (1996), 202–228.
[20] M. Kamei, W. B. Saunders, K. J. Bayless, L. Dye, G. E. Davis and B. M. Weinstein, *Endothelial tubes assemble from intracellular vacuoles*, *in vivo*, Nature, **442** (2006), 453–456.
[21] E. F. Keller and L. A. Segel, *Traveling band of chemotactic bacteria: A theoretical analysis*, Journal of Theo. Biol., **30** (1971), 235–248.
[22] Y. Lei, O. F. Zouani, M. Rémy, L. Ramy and M. C. Durrieu, *Modulation of lumen formation by microgeometrical bioactive cues and migration mode of actin machinery*, Small, In Revision.
[23] Y. Lei, O. F. Zouani, M. Rémy, C. Ayela and M. C. Durrieu, *Geometrical microfeature cues for directing tubulogenesis of endothelial cells*, PLoS ONE, **7** (2012), e41163.
[24] X. D. Liu, S. Osher and T. Chan, *Weighted essentially non-oscillatory schemes*, Journal of Computational Physics, **115** (1994), 200–212.
[25] B. Lubarsky and M. A. Krasnow. *Tube morphogenesis: Making and shaping biological tubes*, Cell, **112** (2003), 19–28.
[26] R. M. Nerem, *Tissue engineering: The hope, the hype, and the future*, Tissue Eng., **12** (2006), 1143–50.
[27] D. V. Nicolau, T. Taguchi, H. Taniguchi, H. Tanigawa and S. Yoshikawa, *Patterning neuronal and glia cells on light-assisted functionalized photoresists*, Biosens. Bioelectron, **14** (1999), 317–325.
[28] Z. K. Otrock, R. A. Mahfouz, J. A. Makarem and A. I. Shamseddine, *Understanding the biology of angiogenesis: Review of the most important molecular mechanisms*, Blood Cells Mol. Dis., **39** (2007), 212–220.
[29] E. M Ouhabaz, "Analysis of Heat Equations on Domains," London Math. Soc. Monographs Series, Princeton University Press. **31**, 2005.
[30] C. S. Patlak, *Random walk with persistence and external bias*, Bull. Math. Biophys., **15** (1953), 311–338.
[31] E. A. Phelps and A. J.Garcia, *Engineering more than a cell: Vascularization strategies in tissue engineering*, Curr. Opin. Biotechnol, **21** (2010), 704–709.
[32] M. I. Santos and R. L. Reis, *Vascularization in bone tissue engineering: Physiology, current strategies, major hurdles and future challenges*, Macromol Biosci., **10** (2010), 12–27.
[33] T. Senba and T. Suzuki, *Chemotactic collapse in a parabolic-elliptic system of mathematical biology*, Adv. Differential Equations, **6** (2001), 21–50.
[34] Y. Y. Li and M. S. Vogelius, *Gradient estimates for solutions to divergence form elliptic equations with discontinuous coefficients*, Arch. Rational Mech. Anal., **153** (2000), 91–151.
[35] F. Y Wang and L.Yan, *Gradient estimate on convex domains and application*, To Appear in AMS. Proc., **141** (2013), 1067–1081. (Avalaible on `http://arxiv.org/abs/1009.1965v2`).

Received June 21, 2012; Accepted April 17, 2013.

E-mail address: `Colin@math.u-bordeaux1.fr`
E-mail address: `marie-christine.durrieu@inserm.fr`
E-mail address: `julie.joie@inria.fr`
E-mail address: `yifeng.lei@inserm.fr`
E-mail address: `youcef.mammeri@u-picardie.fr`
E-mail address: `Clair.Poignard@inria.fr`
E-mail address: `Olivier.Saut@math.u-bordeaux1.fr`